

A coordinate-independent technique for detecting globally inhomogeneous flat topologies (Research Note)

H. Fujii

Institute of Astronomy, School of Science, University of Tokyo, 2-21-1, Osawa, Mitaka, Tokyo 181-0015, Japan

Received / Accepted

ABSTRACT

A flat Universe model supported by recent observations has 18 possible choices for its overall topology. To detect or exclude these possibilities is one of the most important tasks in modern cosmology, but it has been very difficult for globally inhomogeneous ones because of a long-time calculation. In this brief paper we provide an object-based 3D method to overcome the problem, as an extension of Fujii & Yoshii (2011a). Though the test depends on the observer's location in the universe, this method drastically reduces calculation times to constrain inhomogeneous topologies, and will be useful in exhaustively constraining the size of the Universe.

Key words. cosmology: theory - cosmology: large scale structure of Universe

1. Introduction

Theory of modern cosmology is based on Einstein's General Relativity, and recent observations favor a Λ -CDM cosmology with vanishing curvature (e.g., $\Omega_{\text{tot}} = 1.0050^{+0.0060}_{-0.0061}$ from *WMAP*+BAO+SN data, by Hinshaw et al. 2009), which successfully describes the observed properties such as the cosmic structure formation, the cosmic microwave background (CMB) anisotropies, and the accelerating expansion. However, General Relativity does not distinguish two spaces with the same curvature but with different topologies. Though the curvature of our Universe is exactly zero, we still have 18 choices for the overall topology of the Universe (Nowacki 1934), e.g., the multiconnected 3-torus \mathbb{T}^3 with finite volume.

A multiconnected space is a quotient space of the simply connected space with the same curvature (\mathbb{S}^3 , \mathbb{E}^3 , or \mathbb{H}^3), by a holonomy group Γ . An observer in the space would see it as a finite or infinite $2K$ -polyhedron (the *Dirichlet domain*) whose K pairs of faces are glued by the holonomies. There exist the second, third, and more, geodesics between a given object and the observer, which across the Dirichlet domain. As a result, multiple images of single objects, often referred to as "ghosts", can be observed in a multiconnected space (for details, see, e.g., Lachièze-Rey and Luminet 1995).

Based on this prediction, many object-based works for constraining cosmic topology were carried out, i.e., they searched for periodic and symmetrical patterns made by ghosts of galaxies, galaxy clusters, or active galactic nuclei (e.g., Fagundes & Wichoski 1987; Demiański & Łapucha 1987; Lehoucq et al. 1996; Roukema 1996; Uzan et al. 1999; Weatherley et al. 2003; Marecki et al. 2005; Menzies & Mathews 2005). However, their methods are valid only for particular topologies and/or, not sensitive enough to constrain spaces that are comparable to the observed region in size. The method by Roukema (1996) has both the generality and the high sensitivity, but the algorithm is not so sophisticated and the calculations take very long times.

One of the recent trends is to use the *circles-in-the-sky* method (Cornish et al. 1998) that is to search for intersections of the last-scattering surface and the faces of our Dirichlet domain. They appear as circles with the same temperature fluctuation pattern in the CMB map since they are physically identical. This method can detect any topologies, but checking all the possibilities requires an extremely long-time calculation because of the many free parameters: radius of the matched circles and celestial positions of centers of the two circles. Such exhaustive analyses have not carried out yet, and various authors have searched for matched circles limiting to antipodal or nearly antipodal ones, using the *WMAP* satellite's data. However, they obtained diverse results (e.g., Aurich 2008; Roukema et al. 2008; Cornish et al. 2004; Key et al. 2007; Bielewicz & Banday 2011), which suggests that there are methodological problems.

One way to break down this situation is to use observational data that is independent of the CMB observations, e.g., astronomical objects such as galaxies and quasars. This motivates us to revisit the object-based 3D methods, and we developed a method that can constrain any of the 18 flat topologies with simple algorithms, and is much more sensitive to topological signatures than the preceding ones (Fujii & Yoshii 2011a, hereafter FY11a). Nevertheless, it also has a similar problem in checking all the possible topologies: calculation time becomes very long. The aim of this brief paper is to provide a technique to overcome this problem. Throughout the paper we consider flat universes.

2. Method

2.1. Mathematical background and definitions

Mathematical classification of the holonomy groups for flat spaces was completed by Nowacki (1934). Any holonomy γ can be written as $\gamma = \gamma_T \gamma_{NT}$, where γ_T is a parallel translation and γ_{NT} is one of an identity, n -th turn rotations (for $n = 2, 3, 4$, and 6), and a reflection. Those spaces whose holonomy groups include only translations ($\gamma_{NT} = id$) are called (globally) homo-

geneous, otherwise called (globally) inhomogeneous. We investigate the latter topologies in this paper.

We borrow a convenient way of writing the holonomies that is to use a 4D coordinate system (w, x, y, z) where the simply connected 3-Euclidean space \mathbb{E}^3 is represented as a hyperplane $w = 1$, so that a usual 3D vector (x, y, z) is represented as a 4D vector $\mathbf{x} = (1, x, y, z)$. Every holonomy γ is also written as a 4×4 matrix, e.g., a half-turn corkscrew motion is written as:

$$\gamma = U \begin{pmatrix} 1 & 0 & 0 & 0 \\ 0 & -1 & 0 & 0 \\ 0 & 0 & -1 & 0 \\ 0 & 0 & 0 & 1 \end{pmatrix} U^{-1} + \begin{pmatrix} 1 & 0 & 0 & 0 \\ L_1 & 0 & 0 & 0 \\ L_2 & 0 & 0 & 0 \\ L_3 & 0 & 0 & 0 \end{pmatrix},$$

where U is a 4×4 matrix representing the choices of the coordinate systems, which reduces to $U = id$ if we choose our z -axis to be parallel to the rotational axis (hereafter, we call this straight line the *fundamental axis* of the holonomy, denoted by l_{fun}). The unit vector \mathbf{n}_{fun} that is parallel to l_{fun} is called the *fundamental vector*; we identify two antipodal vectors \mathbf{n}_{fun} and $-\mathbf{n}_{fun}$. For a holonomy of reflection, fundamental axis l_{fun} is parallel to the reflectional plane.

In the rest of this paper, unless otherwise stated we continue to consider the same half-turn corkscrew motion as an example.

2.2. Summary of the 3D method of FY11a

In this section we review the FY11a's object-based 3D method for detecting cosmic topology (see the paper for details). Our assumption is that the Universe has the spatial section with zero curvature, as suggested by recent observations. This assumption is also favored by theory of the quantum creation of the universe (Linde 2004).

If a pair of comoving objects \mathbf{x}_1 and \mathbf{x}'_1 are linked by a holonomy γ , we have by definition

$$\mathbf{x}'_1 = \gamma \mathbf{x}_1 = \gamma_T \gamma_{NT} \mathbf{x}_1 = \gamma_{NT} \mathbf{x}_1 + \mathbf{L}, \quad (1)$$

where $\mathbf{L} = (1, L_1, L_2, L_3)$ is the translational vector. Detecting such topological twins requires the parameter searching for 5 parameters: the translational vector \mathbf{L} and the fundamental vector \mathbf{n}_{fun} . To eliminate \mathbf{L} we search for two pairs of ghosts (called a *topological quadruplet*) $[(\mathbf{x}_1, \mathbf{x}_2), (\mathbf{x}'_1, \mathbf{x}'_2)]$ such that

$$\mathbf{x}'_1 = \gamma \mathbf{x}_1 = \gamma_T \gamma_{NT} \mathbf{x}_1 = \gamma_{NT} \mathbf{x}_1 + \mathbf{L}, \quad (2)$$

$$\mathbf{x}'_2 = \gamma \mathbf{x}_2 = \gamma_T \gamma_{NT} \mathbf{x}_2 = \gamma_{NT} \mathbf{x}_2 + \mathbf{L}. \quad (3)$$

Such a quadruplet always satisfies

$$\mathbf{x}'_2 - \mathbf{x}'_1 = \gamma_{NT}(\mathbf{x}_2 - \mathbf{x}_1), \quad (4)$$

independent of \mathbf{L} . If our z -axis is parallel to the fundamental axis l_{fun} (hence $U = id$), the following relations hold:

$$x'_2 - x'_1 = -(x_2 - x_1), \quad (5)$$

$$y'_2 - y'_1 = -(y_2 - y_1), \quad (6)$$

$$z'_2 - z'_1 = z_2 - z_1, \quad (7)$$

since γ is a half-turn corkscrew motion here.

The FY11a's scheme is to search for quadruplets $[(\mathbf{x}_i, \mathbf{x}_j), (\mathbf{x}_k, \mathbf{x}_l)]$ that simultaneously satisfy the following three conditions:

1. separation condition: $|\mathbf{x}_i - \mathbf{x}_j| = |\mathbf{x}_k - \mathbf{x}_l|$.

This condition is common to all holonomies, as holonomies are isometries that preserve distance. Preceding works such as Roukema (1996) and Uzan et al. (1999) also used this mathematical property of holonomies.

2. vectorial condition: eq. (5)-(7).

This is for a half-turn corkscrew motion; for other types of holonomies, see FY11a. Similar condition for a translation was used in Marecki et al. (2005).

3. lifetime condition: $|t_i - t_k|, |t_j - t_l| < t_{life}$.

The variables t_i, t_j, \dots are cosmic times of objects $\mathbf{x}_i, \mathbf{x}_j, \dots$, respectively, and t_{life} is the typical lifetime of objects. This condition is important when considering short-lived objects, e.g., active galactic nuclei.

Due to these multi-filters, only $\lesssim 10$ pairs of ghosts among the total > 1000 objects are sufficient for this test. However, eq. (5)-(7) hold only for the specific coordinate system, so we still have to perform the parameter searching for 2 parameters, the fundamental vector \mathbf{n}_{fun} . To our dismay, this requires over about 10^6 trials that takes a very long time. These strong and weak points of the FY11a's method is seen in Fig 1, where s_i is the number of quadruplets that include the object \mathbf{x}_i as its members and satisfy all the conditions 1-3 (see FY11a for details). When using the z -axis parallel to \mathbf{n}_{fun} , there can be seen some bumps in the histograms that are constituted by topological ghosts, while such bumps are not seen when the z -axis deviates from \mathbf{n}_{fun} . The property of the simulated catalog used here is described in section 3.1.

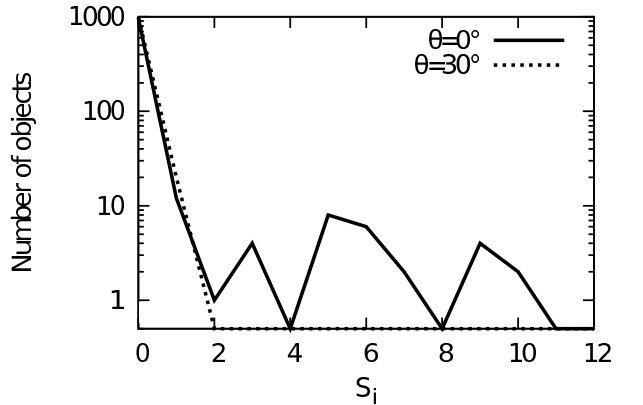


Fig. 1. Solid line: the result using the z -axis parallel to \mathbf{n}_{fun} . Broken line: the result using the z -axis that is at the angle of 30° with \mathbf{n}_{fun} . The vertical scale is linear from 0 to 1 and logarithmic from 1 to 1000. The observer stands at the distance of 3 Gpc from l_{fun} (see section 3.2).

2.3. Fundamental-vector-searching method

One may want to have a coordinate-independent filter to extract topological quadruplets, but it is found to be impossible. Consider an arbitrary quadruplet $[(\mathbf{x}_i, \mathbf{x}_j), (\mathbf{x}_k, \mathbf{x}_l)]$ that already satisfies the separation condition and the lifetime condition. It then also satisfies the vectorial condition eq. (5)-(7) if we choose the z -axis parallel to the vector $\mathbf{a} + \mathbf{b}$, where $\mathbf{a} = \mathbf{x}_j - \mathbf{x}_i$ and $\mathbf{b} = \mathbf{x}_l - \mathbf{x}_k$ (Fig 2). The unit vector $\mathbf{n}_{pec} \propto \mathbf{a} + \mathbf{b}$ is called the *peculiar vector* of the quadruplet, for a half-turn corkscrew motion.

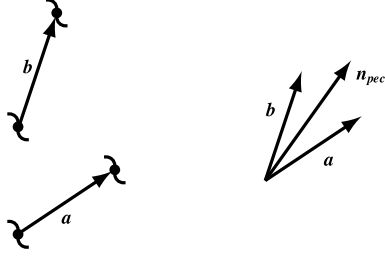


Fig. 2. Even a nontopological quadruplet seems to be linked by a half-turn corkscrew motion when we choose the z -axis parallel to its peculiar axis $\mathbf{n}_{pec} \propto \mathbf{a} + \mathbf{b}$.

Therefore it is impossible to judge whether a given quadruplet is topological, however, if there really exists the fundamental axis (and vector) in the Universe, the number of quadruplets whose peculiar vectors are parallel to it should be larger than stochastically expected. This is the essential idea of the coordinate-independent technique described here. Detailed procedure, hereafter we call the “*fundamental-vector-searching* (FVS)” method, is as follows.

1. The celestial sphere is divided into $12N_{\text{side}}^2$ equal area pixels. Since we identify two antipodal vectors, the number of pixels used is $6N_{\text{side}}^2$.
2. The quadruplets that satisfy both the separation condition and the lifetime condition are selected.
3. For each selected quadruplet, its peculiar vector \mathbf{n}_{pec} and the celestial pixel containing \mathbf{n}_{pec} within it is calculated.
4. For each object \mathbf{x}_i , the pixels containing more than s_{min} peculiar axes of the quadruplets that include \mathbf{x}_i are flagged.
5. Each pixel is assigned an integer, the number of times of being flagged in the previous step.

These steps practically correspond to counting the number of objects with $s_i > s_{\text{min}}$ for all the possible z -axes. Note that the choices of the parameters N_{side} and s_{min} are not independent; a small N_{side} corresponds to large pixels and large stochastic noises, so s_{min} should be chosen to be large enough. HEALPix scheme (Górski et al. 2005) is used in pixelization of the celestial sphere.

We consider the half-turn corkscrew motion as an example throughout this paper, but the treatments on the other types of holonomies are similar except for the step 3. The peculiar axis of the quadruplet $[(\mathbf{x}_i, \mathbf{x}_j), (\mathbf{x}_k, \mathbf{x}_l)]$ for each type of holonomies can be calculated as follows.

1. n -th turn corkscrew motions

In this case the fundamental axis is defined to be parallel to the rotational axis. The apparent angle between \mathbf{a} and \mathbf{b} , therefore, should be $2\pi/n$ when seen from its peculiar vector \mathbf{n}_{pec} . Such a vector is obtained by rotating the unit vector parallel to $\mathbf{a} + \mathbf{b}$ around the axis parallel to $\mathbf{a} - \mathbf{b}$ by the angle of

$$\alpha = \pm \arcsin\left(\frac{\tan \phi}{\tan \frac{\pi}{n}}\right), \quad (8)$$

where ϕ is half the intrinsic angle between \mathbf{a} and \mathbf{b} . The quadruplet with $\phi > \pi/n$ has no peculiar axes, which never occurs when $n = 2$ (half-turn corkscrew motion).

2. glide reflections

In this case the fundamental axis is defined to be perpendicular to the reflectional plane, hence the peculiar vector is the unit vector parallel to $\mathbf{a} - \mathbf{b}$.

3. Simulations and Discussions

3.1. Details of simulated catalog

We generated a full-sky catalog of toy quasars to test the FVS method. The properties of the catalog is given here.

- The standard Λ -CDM cosmology ($\Omega_m = 0.27, \Omega_\Lambda = 0.73, H_0 = 71$ km/sec/Mpc) is used, so that the local geometry is Euclidean.
- A half-turn space topology is assumed, such that the detectable holonomies are only two half-turn corkscrew motions. The translational distance of these detectable holonomies is $L = 10$ Gpc.
- The comoving number density of quasars obeys the empirical law for the luminous quasars (Fan et al. 2001b).
- Quasar luminosity evolution is simplified such that they emit radiation with constant luminosity during the fixed duration $t_{\text{life}} = 10^8$ yr.
- The peculiar motion of quasars is simplified to move with constant speed $v = 500$ km/sec and with randomly chosen directions.
- Other natures of quasars (such as clustering, activity cycle, and anisotropic morphology) and the technical uncertainties are all ignored.

We acknowledge that these simple assumptions are not allowed for practical applications. Simulations in a more realistic situation will be a subject of the coming paper.

3.2. Main results: detection of the fundamental axis

First we applied the FY11a’s method to a toy quasar catalog seen from an observer standing at a comoving distance of 3 Gpc from l_{fun} . The catalog contains 1010 objects at redshifts $z > 4.7$, including 12 pairs of ghosts. Two choices of coordinate systems, $\theta = 0^\circ$ and 30° where θ is the angle between the chosen z -axis and \mathbf{n}_{fun} , were used. These results are given in Fig 1 and already discussed; topological signal appears only for the former case ($\theta = 0^\circ$), and we have to change the z -axis as free parameters to detect globally inhomogeneous topologies (see also section 5.2.1 of FY11a). This takes an extremely long time, and it is our motivation for this work.

Next we applied the FVS method to the same catalog using $N_{\text{side}} = 500$ and $s_{\text{min}} = 2$. If there is a topological quadruplet, its peculiar vector \mathbf{n}_{pec} ideally coincides with the fundamental vector \mathbf{n}_{fun} , but not in practice due to peculiar motions. The resolution parameter N_{side} is determined so as to cover this positional deviations. The cutoff parameter $s_{\text{min}} = 2$ is a reasonable choice because the quadruplets with $s_i > 2$ seem to rarely occur by chance as can be seen in Fig 1.

The results were smoothed and contoured in 2D maps (Fig 3), where the half celestial sphere is orthogonally projected on the xy -plane. As expected, a pixel containing the fundamental axis has larger counts than the other pixels whose counts are purely stochastic, independently of the coordinate systems.

This single calculation takes about a few ten minutes with a present-day ordinary personal computer, and is equivalent to performing about $\sim 10^6$ trials of the FY11a’s method, taking about one year. This is the notable advantage of the FVS method over the other methods, e.g., the CMB-based circles-in-the-sky method that cannot constrain all the possible topologies in a reasonable time.

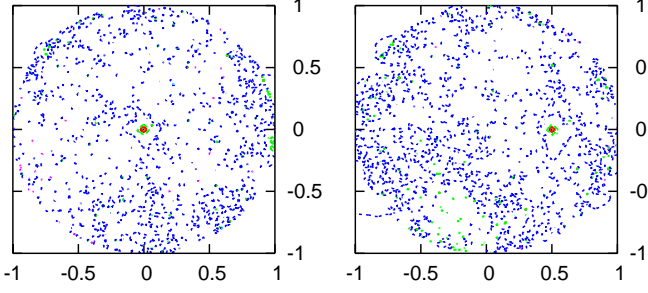


Fig. 3. The fundamental vector \mathbf{n}_{fun} appears as a sharp peak in both cases; left: $\theta = 0^\circ$, right: $\theta = 30^\circ$. The observer stands at the distance of 3 Gpc from the fundamental axis l_{fun} . Plots outside the unit disk are fake made by square-shaped meshing of the region $[-1, 1] \times [-1, 1]$.

3.3. Limits of the method: observer's location

The results of the previous section are based on the somewhat idealized assumptions. In practice, there are various effects to be considered correctly: physical properties of astronomical objects and observational uncertainties. These effects will be treated in the coming papers and not here, however, there is another important factor that affects this test; the limit of the FVS method depends on the observer's location in the universe.

To see this effect, let us consider a topological quadruplet $[(\mathbf{x}_i, \mathbf{x}_j), (\mathbf{x}'_i, \mathbf{x}'_j)]$, which satisfies

$$\mathbf{a}_\perp = -\mathbf{b}_\perp + \boldsymbol{\varepsilon}_\perp, \quad (9)$$

$$\mathbf{a}_\parallel = \mathbf{b}_\parallel - \boldsymbol{\varepsilon}_\parallel, \quad (10)$$

where $\mathbf{a} = \mathbf{x}_j - \mathbf{x}_i$, $\mathbf{b} = \mathbf{x}'_j - \mathbf{x}'_i$, and $\boldsymbol{\varepsilon}$ represents the deviation due to peculiar motions. The lower indices \perp and \parallel represent the vector components perpendicular and parallel to l_{fun} , respectively. The peculiar vector of this quadruplet is

$$\mathbf{n}_{pec} \propto \mathbf{a} + \mathbf{b} \propto \mathbf{n}_{fun} + \frac{\boldsymbol{\varepsilon}_\parallel + \boldsymbol{\varepsilon}_\perp}{2|\mathbf{a}_\parallel|}. \quad (11)$$

If the observer stands near the fundamental axis l_{fun} , the faces of his Dirichlet domain are nearly perpendicular to l_{fun} . On the other hand, ghosts of the short-lived objects such as quasars and starburst galaxies, which are luminous and suitable for high-redshift observations, appear near the faces of the Dirichlet domain. As a result, \mathbf{a}_\parallel becomes small and slight changes in position due to peculiar velocity induce a large deviation of \mathbf{n}_{pec} from \mathbf{n}_{fun} .

Therefore, if the Milky Way is situated near l_{fun} , the FVS method can no longer detect the topological signatures and a troublesome parameter searching is needed. For example, we generated a toy quasar catalog seen from the observer standing along l_{fun} . The catalog contains 1040 objects including 14 pairs of ghosts. In Fig 4, it can be seen that the FVS method does not detect the fundamental vector, while the FY11a's method successfully detects topological signature though in practice a long-time calculation to search for \mathbf{n}_{fun} is needed.

Now we discuss the limitation of the FVS method a little more in detail. In order that there be a sharp peak, both the following conditions must be satisfied:

1. Sufficient number of topological ghosts are in the catalog.
2. All the peculiar vectors \mathbf{n}_{pec} of the topological quadruplets are lying in one (or a few) pixel.

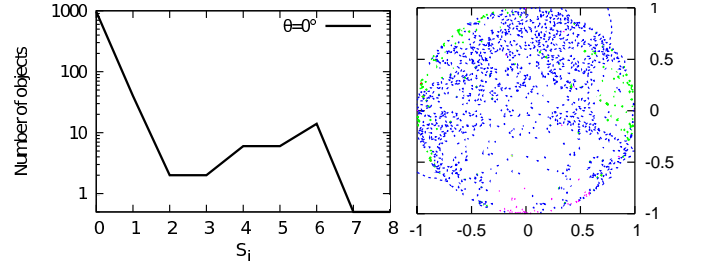


Fig. 4. In the case where the observer stands along l_{fun} , the FVS method does not work well (right), and a tremendous parameter searching of the FY11a's method is necessary (left).

To satisfy the condition 2, the pixel size should be larger than the typical deviation from \mathbf{n}_{fun} of \mathbf{n}_{pec} 's of topological quadruplets, which can be estimated from eq. (11). Then the typical number of \mathbf{n}_{pec} 's of nontopological quadruplets (including a given object \mathbf{x}_i) contained in one pixel can be calculated. The condition 1 claims that this stochastic noise must be sufficiently smaller than the number of topological ghost pairs.

Fig 5 shows the rough estimation of these quantities as a function of r_{obs} , the observer's distance from l_{fun} , in the situation described in section 3.1. The typical size of the universe is fixed to $L = 10$ Gpc for simplicity, though it should be treated as a variable. The FVS method is valid as long as the stochastic noise is small enough compared to the ghost pairs, i.e., $1 \text{ Gpc} \lesssim r_{obs} \lesssim 6 \text{ Gpc}$, which is consistent with the previous results ($r_{obs} = 3 \text{ Gpc}$ and 0 Gpc). When there is no sharp peaks as in Fig 4, we can conclude that $r_{obs} \lesssim 1 \text{ Gpc}$ or $r_{obs} \gtrsim 6 \text{ Gpc}$ for $L = 10 \text{ Gpc}$, and the constraints on r_{obs} for other values of L also can be obtained similarly.

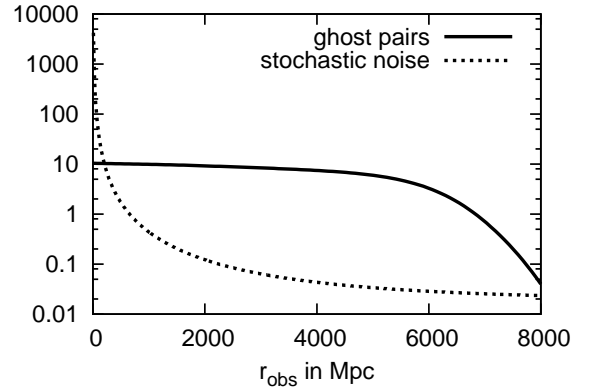


Fig. 5. The FVS method is not valid if stochastic noise $>$ ghost pairs. The universe's typical size is assumed to be $L = 10 \text{ Gpc}$ here.

3.4. Prospects

We introduced the FVS method that, along with the FY11a's method, is useful for constraining topology of the universe with zero curvature. Especially, the former method will provide the first observational constraints on the inhomogeneous topologies, which take an unrealistically long time when using other CMB-based or object-based methods.

However, for practical application we need more realistic simulations. Then our next work will focus on these issues: detailed treatments on physical properties of astronomical ob-

jects and technical uncertainties of observations. When this accomplished, we will be able to apply the FY11a's method and the FVS method to the observed catalogs of our real Universe. Recent and future large-scale survey projects, such as 2dFGRS (Croom et al. 2004), SDSS (Schneider et al. 2010), Large Synoptic Survey Telescope (LSST) and the Joint Astrophysics Nascent Universe Satellite (JANUS), provide sufficient data for this test. Formidable progress in techniques for measuring photometric redshifts suggests that the spectroscopic surveys are not necessarily needed.

Acknowledgements. I gratefully want to thank Y. Yoshii for his various supports, useful discussions and constructive suggestions. I also thank M. Doi, T. Minezaki, T. Tsujimoto, T. Yamagata, T. Kakehata, K. Hattori, and T. Shimizu for useful discussions and suggestions. Some of the results in this paper were derived using the HEALPix package.

References

- Aurich, R. 2008, *Classical and Quantum Gravity*, 25, 225017
 Aurich, R. & Lustig, S. 2011, *Classical and Quantum Gravity*, 28, 085017
 Bielewicz, P. & Banday, A. J. 2011, *MNRAS*, 412, 2104
 Cornish, N. J., Spergel, D. N., & Starkman, G. D. 1998, *Classical and Quantum Gravity*, 15, 2657
 Cornish, N. J., Spergel, D. N., Starkman, G. D., & Komatsu, E. 2004, *Physical Review Letters*, 92, 201302
 Croom, S. M., Smith, R. J., Boyle, B. J., et al. 2004, *MNRAS*, 349, 1397
 Demianski, M. & Lapucha, M. 1987, *MNRAS*, 224, 527
 Fagundes, H. V. & Wichoski, U. F. 1987, *ApJ*, 322, L5
 Fan, X., Strauss, M. A., Schneider, D. P., et al. 2001, *AJ*, 121, 54
 Fujii, H. & Yoshii, Y. 2011a, *A&A*, 529, A121+
 Fujii, H. & Yoshii, Y. 2011b, *A&A*, 531, A171+
 Górski, K. M., Hivon, E., Banday, A. J., et al. 2005, *ApJ*, 622, 759
 Ivezic, Z., Tyson, J. A., Acosta, E., et al. 2008, *ArXiv e-prints*
 Key, J. S., Cornish, N. J., Spergel, D. N., & Starkman, G. D. 2007, *Phys. Rev. D*, 75, 084034
 Lachieze-Rey, M. & Luminet, J. 1995, *Phys. Rep.*, 254, 135
 Lehoucq, R., Lachieze-Rey, M., & Luminet, J. P. 1996, *A&A*, 313, 339
 Lehoucq, R., Uzan, J., & Luminet, J. 2000, *A&A*, 363, 1
 Lew, B. & Roukema, B. 2008, *A&A*, 482, 747
 Linde, A. 2004, *J. Cosmology Astropart. Phys.*, 10, 4
 Marecki, A., Roukema, B. F., & Bajtlik, S. 2005, *A&A*, 435, 427
 Menzies, D. & Mathews, G. J. 2005, *J. Cosmology Astropart. Phys.*, 10, 8
 Mota, B., Rebouças, M. J., & Tavakol, R. 2010, *Phys. Rev. D*, 81, 103516
 Nowacki, W. 1934, *Comment. Math. Helvet.*, 7, 81
 Roming, P. 2008, in *COSPAR, Plenary Meeting*, Vol. 37, 37th COSPAR Scientific Assembly, 2645–+
 Roukema, B. F. 1996, *MNRAS*, 283, 1147
 Roukema, B. F., Buliński, Z., & Gaudin, N. E. 2008a, *A&A*, 492, 657
 Roukema, B. F., Buliński, Z., Szaniewska, A., & Gaudin, N. E. 2008b, *A&A*, 486, 55
 Roukema, B. F., Lew, B., Cechowska, M., Marecki, A., & Bajtlik, S. 2004, *A&A*, 423, 821
 Schneider, D. P., Richards, G. T., Hall, P. B., et al. 2010, *AJ*, 139, 2360
 Uzan, J., Lehoucq, R., & Luminet, J. 1999, *A&A*, 351, 766
 Weatherley, S. J., Warren, S. J., Croom, S. M., et al. 2003, *MNRAS*, 342, L9